1991

Effect of Ohmic, Mass-Transfer, and Kinetic Resistances on Linear-Sweep Voltammetry in a Cylindrical-Pore Electrode

John W. Weidner
University of South Carolina - Columbia, weidner@engr.sc.edu

Peter S. Fedkiw
North Carolina State University at Raleigh

Publication Info

Journal of the Electrochemical Society, 1991, pages 2514-2526.

Publisher's link: http://dx.doi.org/10.1149/1.2086011
DOI: 10.1149/1.2086011

Effect of Ohmic, Mass-Transfer, and Kinetic Resistances on Linear-Sweep Voltammetry in a Cylindrical-Pore Electrode

John W. Weidner*,[1] and Peter S. Fedkiw**

Department of Chemical Engineering, North Carolina State University, Raleigh, NC 27695-7905

ABSTRACT

Extracting quantitative kinetic information from linear-sweep voltammograms (LSV) on porous electrodes is more difficult than on planar electrodes since the electrode surface is not uniformly accessible to the bulk supply of reactant or the counterelectrode. We present here a means to account for the effect of ohmic, mass-transfer, and kinetic resistances on LSV by modeling a pore in a porous matrix as a cylindrical-pore electrode, and solving the mass and charge conservation equations in the context of this geometry for the simply redox reaction $O + ne^- \rightleftharpoons R$ where both O and R are soluble species. Both analytical and numerical techniques are used to solve the governing equations. The calculated peak currents and potentials are correlated by simple-to-apply empirical formulas to the measurable parameters: sweep rate, concentration of the redox species, diffusion coefficient, conductivity of the electrolyte, and pore dimensions. Using the correlations, a methodology is established for determining if the redox reaction kinetics are irreversible or reversible (Nernstian). If the reaction is irreversible, it is shown how the standard rate constant and the transfer coefficient may be extracted from linear-sweep voltammetry data, or if the reaction is reversible, how the number of electrons transferred may be deduced.

Electroanalytical techniques used to study reaction kinetics on planar electrodes do not lend themselves to the study of flooded porous electrodes. For example, hydrodynamic methods [*e.g.*, rotating disk electrodes (1)] are not useful since the reaction surface is inside the porous matrix, and therefore forced convection only affects the material transport to the pore mouth but not within the matrix. In contrast, linear-sweep voltammetry in which the electrolyte is stagnant can be used to perform *in situ* reaction kinetic studies on flooded porous electrodes. However, the presently available mathematical methodologies that have been developed to determine kinetic parameters using LSV on a planar electrode (2-5) and in a thin-layer cell (6-8) are not applicable for a pore except at large and small sweep rates, respectively, and in the absence of appreciable ohmic resistance and axial diffusion. At high sweep rates the diffusion layer is small relative to the pore diameter, and when ohmic resistance is negligible the voltammogram has the characteristics of LSV on a planar electrode. For low sweep rates, radial concentration gradients are small, and if the pore is deep, axial concentration gradients are negligible for the major fraction of the pore volume, and consequently, the pore behaves like a thin-layer cell. However, at moderate sweep rates and/or in the presence of appreciable ohmic resistance and axial diffusion, LSV cannot be characterized by these two limiting cases, and the resulting voltammograms depend on the combined effects of ohmic, mass-transfer, and kinetic resistances.

The approach taken in this paper is to assume a porous electrode is a collection of identical, noninterconnected flooded cylindrical pores. Since all pores are equivalent in this idealized electrode, the behavior of the complete electrode will be the same as that predicted for a single pore. (It is possible to predict the performance for several different pore sizes and then combine the results based on a given pore-size distribution, as suggested by Winsel (9) and de Levie (10).) The reaction occurring is

$$O + ne^- \rightleftharpoons R \qquad [1]$$

where O and R are soluble oxidized and reduced species, respectively, and n is the number of electrons transferred. Using this model, we solved the governing material and charge conservation equations assuming Butler-Volmer kinetics when the potential at the pore opening changes linearly with time. The resulting voltammogram is shown to be a function of six dimensionless parameters. Simple-to-apply empirical correlations which relate the peak currents and potentials to these parameters (or a subset of them) are established from the calculated voltammograms. Numerical solution of the coupled partial differential equations is computer intensive (on the order of one CPU hour per simulation of a voltammogram on an IBM/3090 when using a finite-element technique). Therefore, a parametric evaluation of the general model was conducted by introducing appropriate simplifications at various parameter limits, and only using a finite-element numerical solution of the coupled conservations equations to bridge the gap between the limiting cases.

The nonuniform current distribution problems associated with applying standard LSV methodologies in studying the kinetics of charge transfer at an electrode surface are not confined to porous electrodes. Thin-layer cells or novel analytical techniques like LSV in "holey electrodes" (11) have the limitation that measurements need to be taken in narrow sweep-rate regions where either planar-electrode or thin-layer-cell behavior is observed and under conditions in which ohmic resistance and axial diffusion may be ignored. Although the impetus for our work is to characterize LSV in a porous electrode, the results are applicable to cylindrical-pore electrochemical cells.

Mathematical Model

Assumptions.—A cylindrical pore of diameter d extends from $z = 0$ to L. At the pore aperture ($z = 0$), the tube is exposed to the bulk solution containing both oxidized species O and reduced species R. The potential at the inlet of the tube is potentiostatically controlled. The inner wall of the tube is electroactive, and the closed end ($z = L$) is inactive. Other assumptions are:

1. The solid phase is isopotential.
2. The reaction is a simple redox process with soluble reactant and product.
3. No other processes limit or alter the rates of mass transfer and charge transfer (*i.e.*, no adsorption or desorption and no preceding or following chemical reactions).
4. The solution-phase potential is governed by Laplace's equation.
5. Diffusion is the dominant mass-transfer mechanism.
6. The diffusion coefficients for the two reacting species are equal ($\mathcal{D}_O = \mathcal{D}_R = \mathcal{D}$).
7. The reference electrode is placed at the pore aperture.
8. Nonfaradaic current is negligible.
9. The electrolyte in the reservoir is stagnant, and the axial concentration gradient of the reacting species at the pore opening is proportional to the difference between the bulk and aperture concentrations.
10. The potential is radially uniform at the pore aperture.

Assumptions 1-5 are common to most models of porous electrodes, although some, such as that of Grens and Tobias (12, 13), include the effects of migration and variable conductivity. Grens (14) addresses the importance of these

* Electrochemical Society Student Member.
** Electrochemical Society Active Member.
[1] Present address: Department of Chemical Engineering, University of South Carolina, Columbia, South Carolina 29208.

and other assumptions for the prediction of steady-state current density with a one-dimensional model.

The assumption of equal diffusivities (assumption 6) eliminates the diffusion equation for one of the redox species. In a previous study (5) we included the effect of differing diffusion coefficients in the calculations for LSV on a planar electrode with reversible redox kinetics. For a cathodic sweep when the diffusion coefficient of the reduced species was 50% higher than that of the oxidized species (a significant variation), the peak current was less than 2% greater, and the peak potential $5/n$ mV (T = 298 K) more negative than if the diffusion coefficients were equal. If the kinetics are irreversible, the concentration distribution of only the reactant is important, and assumption 6 has no effect on the voltammogram. Neglecting uncompensated resistance (assumption 7) limits the usefulness of the results if the potential drop between the reference electrode and the pore aperture is appreciable since the sweep rate at the pore opening would no longer be linear. However, uncompensated resistance may be negligible even when ohmic losses inside the pore are appreciable if the cross-sectional area available for current flow is larger outside the pore than inside and the distance from the reference electrode to the pore mouth is small. Neglecting double-layer charging (assumption 8) places a lower limit on the reactant concentration since only the reaction current decreases with a decreasing concentration, and an upper limit on the sweep rate since the charging current is a stronger function of the sweep rate than is the reaction current. The restrictions on the reactant concentration and the sweep rate though are of the same order of magnitude as those for LSV on a planar electrode (1).

Assumption 9 is an attempt to account for mass-transfer resistance in the bulk electrolyte by conceptualizing the pore aperture as an electroactive disk embedded on an insulating plane. Using this same approximation, Bond *et al.* (15) calculated the rate of diffusion of the reacting species into a cylindrical pore in which the closed end was electroactive and the walls were inactive. Assumptions 9 and 10 are invoked since a rigorous treatment which would eliminate these two assumptions would require the simultaneous solution of the governing equations inside and outside the tube, a fairly intractable problem.

Governing equations.—The concentration of the oxidized species is governed by the time-dependent, two-dimensional diffusion equation which in dimensionless form is

$$\frac{\partial C_O^*}{\partial \tau} = \frac{\partial^2 C_O^*}{\partial Z^2} + \frac{1}{Y}\frac{\partial}{\partial Y}\left(Y\frac{\partial C_O^*}{\partial Y}\right) \qquad [2]$$

where the dimensionless variables are defined in the notation section. The following boundary conditions reflect the model assumptions

$$\tau = 0; \quad C_O^* = 1 \qquad [2a]$$

$$Z = 0; \quad \frac{\partial C_O^*}{\partial Z} = \left(\frac{4}{\pi}\right)(C_O^* - 1) \qquad [2b]$$

$$Z = \gamma; \quad \frac{\partial C_O^*}{\partial Z} = 0 \qquad [2c]$$

$$Y = 0; \quad \frac{\partial C_O^*}{\partial Y} = 0 \qquad [2d]$$

$$Y = 1; \quad \frac{\partial C_O^*}{\partial Y} = -\sqrt{\sigma} I^* \qquad [2e]$$

where the dimensionless parameters are defined in Table I, and I^* is the dimensionless local reaction current density, which is positive for a cathodic reaction. For reactions in which the kinetics are governed by the Butler-Volmer rate equation, I^* is given by

$$I^* = \Lambda\left[C_O^* e^{-\alpha E_W^*} - \left(\frac{1 + \xi - \xi C_O^*}{\xi}\right) e^{(1-\alpha)E_W^*}\right] \qquad [3]$$

Table I. Definition of the dimensionless parameters that govern LSV in a cylindrical-pore electrode and physical interpretation. The first three parameters have been used previously for LSV on a planar electrode, where Λ and α are applicable for irreversible kinetics (3, 4) and ξ is applicable for reversible kinetics (5).

Parameter	Interpretation	Definition
Λ	$\frac{\text{Mass-transfer resistance}}{\text{Kinetic resistance}}$	$\frac{k^o}{(nf\nu\mathcal{D})^{1/2}}$
α	Cathodic transfer coefficient	
ξ	Initial concentration ratio	C_O^o/C_R^o
σ	$\frac{\text{Diffusion time}}{\text{Sweep time}}$	$\frac{d^2 nf\nu}{4\mathcal{D}}$
Θ	$\frac{\text{Ohmic resistance}}{\text{Mass-transfer resistance}}$	$\frac{2n^{5/2}F f^{3/2} L^2 C_O^o (\nu\mathcal{D})^{1/2}}{d\kappa}$
γ	$\frac{\text{Length}}{\text{Radius}}$	$\frac{2L}{d}$

where Eq. [3] makes use of the assumption of equal diffusivities for which the dimensionless concentration of the oxidized and reduced species are related by the mass balance

$$1 + 1/\xi = C_O^*(Z, Y, \tau) + C_R^*(Z, Y, \tau) \qquad [4]$$

Laplace's equation governs the difference between the electrode and solution potential E which in dimensionless form is

$$0 = \frac{\partial^2 E^*}{\partial Z^2} + \frac{1}{Y}\frac{\partial}{\partial Y}\left(Y\frac{\partial E^*}{\partial Y}\right) \qquad [5]$$

with boundary conditions

$$Z = 0; \quad E^* = \ln \xi - \sigma\tau \qquad [5a]$$

$$Z = \gamma; \quad \frac{\partial E^*}{\partial Z} = 0 \qquad [5b]$$

$$Y = 0; \quad \frac{\partial E^*}{\partial Y} = 0 \qquad [5c]$$

$$Y = 1; \quad \frac{\partial E^*}{\partial Y} = (\Theta/\gamma^2) I^* \qquad [5d]$$

Since each finite-element simulation of a voltammogram takes on the order of one CPU hour on an IBM/3090, it is desirable to make some simplifications. Figure 1 contains a schematic of the simplifications made in this work which decrease the number of parameters influencing the voltammogram. For instance, the concentration ratio ξ is not applicable for irreversible kinetics, and the ratio of kinetic to mass-transfer resistance Λ does not apply for reversible kinetics. The length-to-radius ratio γ is eliminated when axial diffusion is negligible, regardless of whether or not ohmic resistance is appreciable, and the ratio of ohmic resistance to mass-transfer resistance Θ is only applicable when ohmic resistance is appreciable.

Correlations are obtained in the limit of irreversible and reversible kinetics when axial diffusion is negligible. When ohmic resistance is negligible, the peak currents and potentials are correlated to Λ, α, and σ for irreversible kinetics, and to ξ and σ for reversible kinetics. In the presence of appreciable ohmic resistance, the additional parameter Θ is incorporated into the correlations. Due to the requisite computer time, the correlation for the case when the kinetics are reversible and ohmic resistance is appreciable is established at large ξ, for which the voltammogram becomes independent of this parameter. Also presented are the criteria for which axial diffusion and ohmic resistance may be ignored.

Negligible axial diffusion: With and without appreciable ohmic resistance.—The axial component of Eq. [2] may

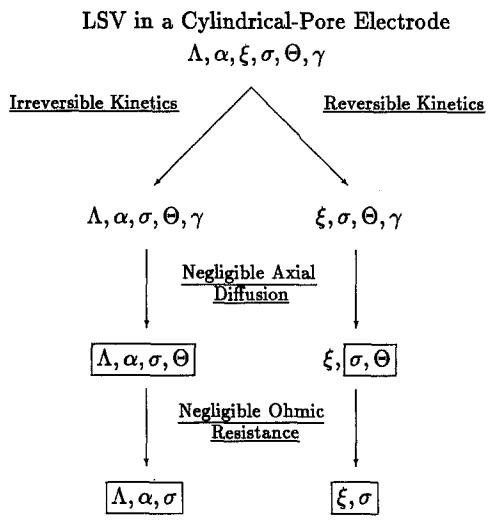

Fig. 1. Schematic of the simplifications made in this work and the resulting parameters that govern LSV in a cylindrical-pore electrode. Correlations are obtained for the peak currents and potentials as a function of the parameters which are boxed in the limit of irreversible and reversible kinetics when axial diffusion is negligible. Due to the requisite computer time, the correlation for the case when the kinetics are reversible and ohmic resistance is appreciable is obtained at large ξ for which the voltammogram becomes independent of this parameter. Also presented in this work are the criteria for which axial diffusion and ohmic resistance may be ignored.

be eliminated when axial diffusion is negligible. The Laplace transform of the resulting equation is taken with respect to τ, the resulting ordinary differential equation for the transformed concentration is solved, the gradient of the transformed concentration at the electrode surface is related to the transformed reaction current, and finally the convolution property of Laplace transforms is applied to invert back to the time domain resulting in

$$C_O^*(1,\tau) = 1 - 2\sqrt{\sigma}\int_0^\tau \left[1 + \sum_{n1=1}^{\infty} e^{-\lambda_{n1}^2(\tau-\tau')}\right] I^*(\tau')d\tau' \quad [6]$$

where λ_{n1} are the zeros of the first-order Bessel function $J_1(\lambda_{n1}) = 0$.

Equation [6] is valid regardless of the particular form of the reaction rate equation since it relates the concentration of O at the electrode surface to an, as yet, unspecified reaction current. In order to generate a voltammogram, it is necessary to determine the current at every point in the sweep. As a step in calculating $I^*(\tau)$, the integral in Eq. [6] is approximated numerically (2) as

$$\int_0^\tau \left[1 + \sum_{n1=1}^{\infty} e^{-\lambda_{n1}^2(\tau-\tau')}\right] I^*(\tau')d\tau' \approx \sum_{\mu=0}^{q-1} B_\mu I^*(qh - \mu h) \quad [7]$$

where h is the interval width such that $\tau = qh$ and $\tau' = \mu h$. The coefficient B_μ are determined by approximating the unknown function $I^*(\tau')$ by a linear expression in the interval between μ and $\mu - 1$, integrating the left side of Eq. [7], and solving for the coefficients. For $\mu = 0$ this procedure results in

$$B_0 = \frac{h}{2} - \sum_{n1=1}^{\infty}\left(\frac{1 - e^{-\lambda_{n1}^2 h} - \lambda_{n1}^2 h}{\lambda_{n1}^4 h}\right) \quad [8]$$

and for μ from 1 to $q - 1$

$$B_\mu = h + \sum_{n1=1}^{\infty} \frac{e^{-\lambda_{n1}^2 h(\mu-1)}}{\lambda_{n1}^4 h}(1 - e^{-\lambda_{n1}^2 h})^2 \quad [9]$$

(Richardson extrapolation (16) was used to speed the convergence of Eq. [8] and [9] and all other nonoscillating series given in this paper.)

If ohmic resistance is negligible, the potential at the tube wall E_w^* is equal to that applied at the pore opening ($E_w^* = \ln \xi - \sigma\tau$), but in the presence of appreciable ohmic resistance, the two-dimensional form of Laplace's equation for the potential (Eq. [5]) must be solved to obtain E_w^*. Winsel (9) and Viner and Fedkiw (17) solved Eq. [5] to determine E_w^* as a function of axial position for an arbitrary time-dependent potential variation at the pore opening. For a linear potential ramp ($-\sigma\tau$), the wall potential at any axial position and time is

$$E_w^*(Z,\tau) = -\sigma\tau + \left(\frac{2\Theta}{\gamma^3}\right)\sum_{n=1}^{\infty}\frac{I_0(\beta_n)}{\beta_n I_1(\beta_n)}\sin\beta_n Z\int_0^\gamma I^*(Z',\tau)\sin\beta_n Z' dZ' \quad [10]$$

where $I_0(\beta_n)$ and $I_1(\beta_n)$ are zero- and first-order modified Bessel functions, respectively, and $\beta_n \equiv (n - \frac{1}{2})\pi/\gamma$. Equation [10] is valid regardless of the reaction rate equation. Although Eq. [10] is a function of γ, it can be shown that in the limit of $\gamma \to \infty$, Eq. [10] is independent of γ. Further, the results presented here which make use of Eq. [10] were independent of γ for $\gamma \geq 10$ within the accuracy of the solution methods employed. Therefore, in the limit of negligible axial diffusion the voltammogram is independent of γ for $\gamma \geq 10$.

Quasi-reversible kinetics.—Substituting Eq. [6] and [7] into Eq. [3] and solving for the current gives

$$I_{qrev}^*(qh) = \frac{\Lambda\left[\left(1 - 2\sqrt{\sigma}\sum_{\mu=1}^{q-1} B_\mu I_{qrev}^*(qh - \mu h)\right)(1 + e^{E_w^*}) - (1 + 1/\xi)e^{E_w^*}\right]}{e^{\alpha E_w^*} + 2\sqrt{\sigma}\Lambda B_0(1 + e^{E_w^*})} \quad [11]$$

where the subscript "qrev" indicates quasi-reversible kinetics. The voltammogram is obtained by stepping Eq. [11] through time with $E_w^* = (\ln \xi - \sigma\tau)$ when ohmic resistance is negligible, or coupling it with Eq. [10] in the presence of appreciable ohmic resistance.

Irreversible kinetics.—When the kinetics are irreversible Eq. [3] reduces to

$$I_{irrev}^* = \Lambda C_O^* e^{-\alpha E_w^*} \quad [12]$$

where the subscript "irrev" indicates irreversible kinetics. Substituting Eq. [6] and [7] into Eq. [12] and solving for $I_{irrev}^*(qh)$ gives

$$I_{irrev}^*(qh) = \frac{\Lambda\left[1 - 2\sqrt{\sigma}\sum_{\mu=1}^{q-1} B_\mu I_{irrev}^*(qh - \mu h)\right]}{e^{\alpha E_w^*} + 2\sqrt{\sigma}\Lambda B_0} \quad [13]$$

Reversible kinetics.—For a reversible electrochemical reaction, the surface concentrations of O and R are coupled through the Nernst equation to the potential by

$$C_O^*(1,\tau) = \frac{(1 + \xi)e^{E_w^*}}{\xi[1 + e^{E_w^*}]} \quad [14]$$

Substituting Eq. [6] and [7] into Eq. [14] and solving for the current gives

$$I_{rev}^*(qh) = \frac{\xi - e^{E_w^*}}{2\xi\sqrt{\sigma}B_0[1 + e^{E_w^*}]} - \sum_{\mu=1}^{q-1} B_\mu I_{rev}^*(qh - \mu h)/B_0 \quad [15]$$

where the subscript "rev" denotes reversible kinetics.

In order to assess the accuracy of the integral approximation given in Eq. [7], an alternative solution to the time and radial-dependent diffusion equation can be generated when the kinetics are reversible by solving the equation for a unit step change in the potential at the tube wall and using Duhamel's superposition principle [18] to account for the time-dependent boundary condition given by Eq. [14]. The resulting expression is

$$I^*_{rev}(\tau) = 2(1 + \xi)\sqrt{\sigma} \sum_{n0=1}^{\infty} \int_0^{\tau} \frac{\exp\left[-[\sigma\tau' + \lambda_{n0}^2(\tau - \tau')]\right]}{[1 + \xi \exp(-\sigma\tau')]^2} d\tau' \quad [16]$$

where λ_{n0} are the zeros of the zero-order Bessel function $J_0(\lambda_{n0}) = 0$.

Results and Discussion

As outlined in Fig. 1, correlations are obtained in the limit of irreversible and reversible kinetics for the peak currents and potentials as a function of the governing dimensionless parameters when axial diffusion is negligible. Equations [13] and [15] are applied for irreversible and reversible kinetics, respectively, with $E^*_w = (\ln \xi - \sigma\tau)$ when ohmic resistance is negligible or coupled with Eq. [10] when it is appreciable. Equations [2] and [5] are solved simultaneously in parameter regions where the iterative technique used to couple the analytical expressions does not converge and to establish the criteria for neglecting axial diffusion. Computational details and the computer codes are available in the thesis upon which this work is based (19).

Negligible ohmic resistance and axial diffusion.—Irreversible kinetics.—When the kinetics are irreversible, it was shown that on a planar electrode (2-4) and in a thin-layer cell (7) the quantities $(I^*_{p,irrev}/\sqrt{\alpha})$ and $[\alpha E^*_{p,irrev} - \ln(\Lambda/\sqrt{\alpha})]$ are a function only of the product of the dimensionless sweep rate and the transfer coefficient, $\alpha\sigma$. The voltammogram for LSV in a cylindrical-pore electrode when the kinetics are irreversible and ohmic resistance and axial diffusion are negligible also depends only upon $\alpha\sigma$ if the voltammogram is plotted as shown in Fig. 2. The voltammograms in Fig. 2 are at three values of $\alpha\sigma$ and result from the application of Eq. [13] with $E^*_w = (\ln \xi - \sigma\tau)$.

In order to illustrate the linear asymptote in the peak current at small $\alpha\sigma$, the dimensionless peak values obtained by applying Eq. [13] are plotted in Fig. 3 as a function of $\sqrt{\alpha\sigma}$. Only the simulation data up to $\sqrt{\alpha\sigma} = 20$ are shown to emphasize the transition in the behavior of the peak values between large and small $\alpha\sigma$. As $\alpha\sigma \to \infty$, the diffusion layer is small relative to the pore diameter, and the peak values approach those obtained for LSV on a planar electrode [*i.e.*, the peak current is proportional to the square root of the sweep rate, and the peak potential shifts $30/n\alpha$ mV at $T = 298$ K for every tenfold increase in the sweep rate (2-4)]. The peak currents and potentials for LSV on a planar electrode are listed in rows 1 and 2 of Table II along with the lowest value of $\alpha\sigma$ for which this limit reasonably holds in a cylindrical-pore electrode. That is, the peak currents for LSV on a planar electrode are within 5% of those obtained in a cylindrical-pore electrode for $\alpha\sigma > 225$, and the peak potentials are within $5/n\alpha$ mV ($T = 298$ K) of each other for $\alpha\sigma > 45$.

As the sweep rate approaches zero ($\alpha\sigma \to 0$), the radial concentration gradients approach zero, and the voltammograms have the characteristics of LSV in a thin-layer cell [*i.e.*, the peak current is proportional to the sweep rate, and the peak potential shifts $59/n\alpha$ mV at $T = 298$ K for every tenfold increase in the sweep rate (7)]. The peak currents and potentials for LSV in a thin-layer cell are listed in rows 3 and 4 of Table II along with the highest value of $\alpha\sigma$ for which this limit holds in a cylindrical-pore electrode.

In order to correlate the peak values to $\alpha\sigma$ over the entire parameter range, the following empirical relationships, motivated by the asymptotic trends seen in Fig. 3, were fit to the peak currents and potentials obtained from Eq. [13]

$$I^*_{p,irrev}(\alpha\sigma) = [I^*_{p,irrev}(\text{planar})^m + I^*_{p,irrev}(\text{thin-layer})^m]^{1/m} \quad [17]$$

where $m = -1.81$, and

$$\exp \alpha E^*_{p,irrev}(\sigma) = [(\exp \alpha E^*_{p,irrev}(\text{planar}))^m + (\exp \alpha E^*_{p,irrev}(\text{thin-layer}))^m]^{1/m} \quad [18]$$

where $m = 2.05$. The empirically determined m values were found by least squares fit of the above equations to the peak values for 250 different values of $\alpha\sigma$ with σ ranging from 10^{-1} to 10^4 and α ranging from 0.1 to 0.9. Equations [17] and [18] are plotted on Fig. 3 as the solid lines and are seen to fit the calculations well.

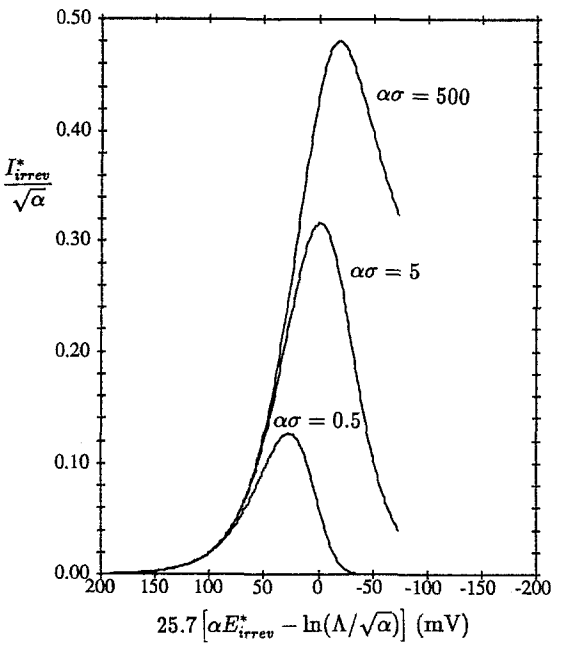

Fig. 2. Illustration of the effect of the product of the dimensionless sweep rate and the transfer coefficient, $\alpha\sigma$, on the calculated cathodic voltammograms for linear-sweep voltammetry in a cylindrical-pore electrode. The simulations result from applying Eq. [13] with $E^*_w = (\ln \xi - \sigma\tau)$ for which the kinetics are irreversible, and ohmic resistance and axial diffusion are negligible. At $\alpha\sigma = 500$, the peak current is approximately 3% less than that on a planar electrode and $1/n\alpha$ mV more positive. At $\alpha\sigma = 0.5$, the voltammogram approaches that obtained in a thin-layer cell with the peak current approximately 3% lower and the peak potential $0.5/n\alpha$ mV more positive. The potential, in mV, is for $T = 298$ K.

Aoki *et al.* (20) also used the peak values for LSV on a planar electrode (3, 4) and in a thin-layer cell (6) as asymp-

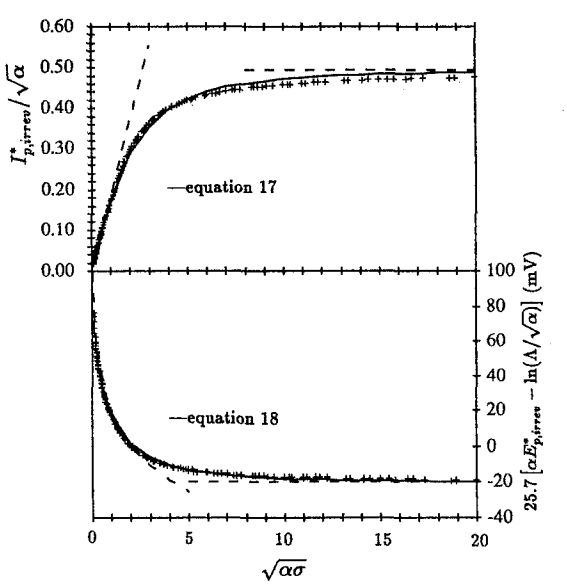

Fig. 3. Calculated dimensionless peak currents and potentials for linear-sweep voltammetry in a cylindrical-pore electrode when the kinetics are irreversible and ohmic resistance and axial diffusion are negligible. The symbols result from the use of Eq. [13] with $E^*_w = (\ln \xi - \sigma\tau)$ and the solid lines are the correlations which were fit to the calculations. The dashed lines as $\alpha\sigma \to \infty$ are the dimensionless peak currents and potentials for LSV on a planar electrode (2-4), and those as $\alpha\sigma \to 0$ are for LSV in a thin-layer cell (7) (see Table II). The potential is for $T = 298$ K.

Table II. Expressions for the peak current and potential on a planar electrode and in a thin-layer cell for irreversible kinetics. The $\alpha\sigma$ limit column indicates the value at which the peak currents are within 5% and the peak potentials within $5/n\alpha$ mV (T = 298 K) of the values calculated for LSV in a cylindrical-pore electrode if ohmic resistance and axial diffusion are negligible.

Peak current or potential expression	Reference	$\alpha\sigma$ Limit
$I^*_{p,irrev}(\text{planar}) = 0.4958\sqrt{\alpha}$	(2-4)	$\alpha\sigma > 225$
$E^*_{p,irrev}(\text{planar}) = \frac{1}{\alpha}\left[\ln\left(\frac{\Lambda}{\sqrt{\alpha}}\right) - 0.780\right]$	(2-4)	$\alpha\sigma > 45$
$I^*_{p,irrev}(\text{thin-layer}) = 0.184\,\alpha\sqrt{\sigma}$	(7)	$\alpha\sigma < 1$
$E^*_{p,irrev}(\text{thin-layer}) = \frac{1}{\alpha}\left[\ln\left(\frac{\Lambda}{\sqrt{\alpha}}\right) - \ln\left(\frac{\sqrt{\alpha\sigma}}{2}\right)\right]$	(7)	$\alpha\sigma < 12$

totic limits at large and small sweep rates, respectively, to obtain two-parameter empirical fits of the peak currents and potentials for LSV in a rectangular cell when the kinetics are reversible and ohmic resistance and axial diffusion are negligible. Daruházi *et al.* (21) confirmed experimentally the transition between planar-electrode and thin-layer-cell behavior from voltammograms generated in a rectangular cell.

Methodology to extract kinetic constants for an irreversible reaction.—Equations [17] and [18] are made dimensional by substituting in the planar-electrode and thin-layer-cell limiting expressions from Table II along with the definitions for σ and I^* (with the total current $i = AI$ where A is the electrode area, and the "Λ" symbol indicates what would be measured if ohmic resistance and axial diffusion were negligible). The resulting dimensional peak-current equation shows that the transfer coefficient α can be estimated from either the slope or intercept of a $(\nu/i_p)^{1.81}$ *vs.* $\nu^{0.905}$ plot. (See first three rows of Table III.) After α is determined, the standard rate constant k° can be estimated from either the slope or intercept of a $(\nu e^{\alpha \hat{E}^*_p})^{2.05}$ *vs.* $\nu^{1.025}$ plot.

If all the data are close to the planar-electrode limit, the intercept will be small relative to the slope times the abscissa, and the kinetic constants obtained from the slope should be a better estimate than those obtained from the intercept. However, if the sweep rates are low such that most of the data lie in the thin-layer-cell limit, the reverse of that stated above will be true. For data in the transition region between the two limits, an average of the estimation from the slope and the intercept is recommended.

The utility of this procedure was evaluated by choosing a set of values for all system variables, including α and k°, using 30 simulation LSV data for which σ varied from 0.1 to 1000, and then calculating α and k° from the slope and intercept of the appropriate plot. Table III lists the system variables, the calculated kinetic parameters, and the absolute percent deviation between the actual and calculated values of α and k°. The majority of the data lie in the transition region between the planar-electrode and thin-layer-cell limits, and as expected the slope and intercept give an estimate of the kinetic parameters to within the same percent deviation, with the average of the two usually resulting in an even more accurate estimate. The average of α(slope) and α(intercept) was used along with the peak potentials to determine k°. Although Table III indicates that α and k° may be estimated to within the same percent deviation, in practice the uncertainty in k° will probably be greater since the experimental uncertainty in the peak potentials is greater than that for the peak currents. The peak potentials from the simulations were recorded to $\pm 1/n\alpha$ mV (T = 298 K), which translates into an 8% error in the ordinate values given in Table III. From Fig. 2 we see that graphically the uncertainty in the potential could be $\pm 5/n\alpha$ mV (T = 298 K), which is an uncertainty in the ordinate value of 50%. Although this uncertainty is significant, the error is of the same magnitude as that arising from LSV on a planar electrode, and the resulting estimate of k° is usually sufficient.

Reversible kinetics.—When the kinetics are reversible, it was shown that on a planar electrode $I^*_{p,rev}$ and $E^*_{p,rev}$ are independent of σ (3-5) but do depend upon ξ (5). In a thin-layer cell it was shown that $I^*_{p,rev}$ is a linear function of $\sqrt{\sigma}$, and $E^*_{p,rev}$ is independent of σ (6). Here we show how the functional dependence of the peak value on σ given by Hubbard and Anson (6) can be extended to include a ξ dependence. The voltammogram for LSV in a cylindrical-pore electrode when the kinetics are reversible and ohmic resistance and axial diffusion are negligible also depends only upon σ and ξ.

In order to illustrate the linear asymptote in the peak current which depends on ξ, the dimensionless peak values obtained by applying Eq. [15] with $E^*_w = (\ln \xi - \sigma\tau)$

Table III. The suggested manner to plot LSV data from a cylindrical-pore electrode for an irreversible reaction in order to extract kinetic constants. As an illustration, the agreement of simulation results with the empirical fit is presented assuming: n = 1, T = 298 K, d = 0.02 cm, L = 0.3 cm, C°_O = 10^{-5} mol/cm^3, $\mathcal{D}$ = 10^{-5} cm^2/s, k° = 10^{-8} cm/s, and 0.25 mV/s $\le \nu \le$ 2.5 V/s. With this data, σ ranges from 0.1 to 1000. The "Λ" symbol above the peak current and potential indicates what would be measured if ohmic resistance and axial diffusion were negligible. First α was determined from the peak currents, and then the average of α(slope) and α(intercept) was used along with the peak potentials to determine k°.

Plot	$\left(\frac{\nu}{i_p}\right)^{1.81}$ *vs.* $\nu^{0.905}$	$(\nu e^{\alpha \hat{E}^*_p})^{2.05}$ *vs.* $\nu^{1.025}$
Slope	$(1.56nFdLC^\circ_O\sqrt{\alpha nf\mathcal{D}})^{-1.81}$	$\left(\frac{0.458k^\circ}{\sqrt{\alpha nf\mathcal{D}}}\right)^{2.05}$
Intercept	$(0.289n^2fFd^2LC^\circ_O\alpha)^{-1.81}$	$\left(\frac{4k^\circ}{\alpha nfd}\right)^{2.05}$

α (Actual)	α (Slope)	|%| Dev.	α (Intercept)	|%| Dev.	$k^\circ \times 10^8$ cm/s (slope)	|%| Dev.	$k^\circ \times 10^8$ cm/s (intercept)	|%| Dev.
0.1	0.096	4	0.100	<1	1.02	2	1.00	<1
0.3	0.293	2	0.288	4	1.01	1	1.00	<1
0.5	0.475	5	0.516	3	1.01	1	0.97	3
0.7	0.667	5	0.716	2	1.03	3	0.95	5
0.9	0.861	4	0.914	2	1.05	5	0.95	5

are plotted in Fig. 4 as a function of $\sqrt{\sigma}$ for three values of ξ. Only a portion of the calculated results are shown in order not to clutter the figure and to emphasize the transition in the behavior between large and small σ. As with irreversible kinetics, the peak values approach those obtained for LSV on a planar electrode as $\sigma \rightarrow \infty$ (*i.e.*, the peak current is proportional to the square root of the sweep rate, and the peak potential is sweep-rate independent). We previously developed correlations for the peak currents and potentials as a function of ξ for LSV on a planar electrode (5) based upon the results of Matsuda and Ayabe (3) and Nicholson and Shain (4), and these are listed in rows 1 and 2 of Table IV. The first two elements of the last column in this table show the lowest value of σ for which planar-electrode behavior reasonably holds for a cylindrical-pore electrode; that is, the peak currents for LSV on a planar electrode are within 5% of those obtained in a cylindrical-pore electrode for $\sigma > 300$, and the peak potentials are within $5/n$ mV ($T = 298$ K) for $\sigma > 40$.

As the sweep rate approaches zero, the voltammograms have the characteristics of LSV in a thin-layer cell (*i.e.*, the peak current is proportional to the sweep rate and the peak potential is sweep-rate independent). Hubbard and Anson (6) derived a current-potential relationship for LSV in a thin-layer cell when only the oxidized species is initially present ($\xi = \infty$) and the voltage is swept cathodically. They found that the cathodic current density is given by

$$I_{rev}(\text{thin-layer}) = \frac{n^2 f F V C_O^\circ \nu e^{E^*}}{A[1 + e^{E^*}]^2} \qquad [19]$$

where V is the volume of the thin-layer cell. When the initial concentration of the reduced species is not negligibly small, Eq. [19] remains valid except that C_O° is replaced by $(C_O^\circ + C_R^\circ)$. Therefore, when $C_O^\circ > C_R^\circ$ ($\xi > 1$), the peak is the formal potential ($E_p^* = 0$) for all values of ξ. However, when $C_O^\circ < C_R^\circ$ ($\xi < 1$) the starting potential is negative with respect to the formal potential and therefore the peak current occurs at the start of the sweep ($E_p^* = \ln \xi$) and the current decays monotonically as the oxidized species is reduced. The dimensionless peak values in the limit of $\sigma \rightarrow 0$ are listed in rows 3 and 4 of Table IV.

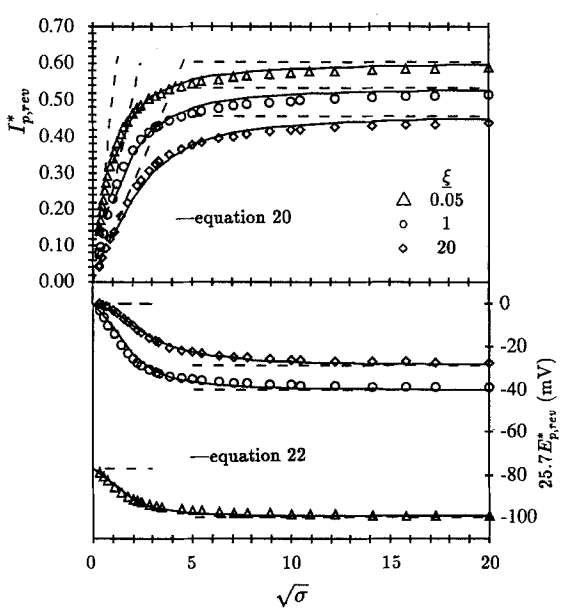

Fig. 4. Calculated dimensionless peak currents and potentials for linear-sweep voltammetry in a cylindrical-pore electrode when the kinetics are reversible and ohmic resistance and axial diffusion are negligible. The symbols result from the use of Eq. [15] with $E_w^* = (\ln \xi - \sigma\tau)$ and the solid lines are the correlations which were fit to the calculations. The dashed lines as $\sigma \rightarrow \infty$ are the dimensionless peak currents and potentials for LSV on a planar electrode (5), and those as $\sigma \rightarrow 0$ are for LSV in a thin-layer cell (6) (see Table IV). The potential is for $T = 298$ K.

The highest value of σ for which thin-layer-cell behavior is observed is a strong function of ξ. For $\xi \geq 5$, the peak current obtained froim Eq. [15] is within 5% of $I^*_{p,rev}$(thin-layer) given in Table IV when $\sigma < 2$, but for $\xi \leq 0.1$, σ has to be less than 0.1 for the two currents to be within 5%. A functional dependence of the upper σ limit on ξ was obtained by performing a two-parameter empirical fit shown in row 3 of Table IV. Hubbard and Anson (6) gave the upper limit on σ as 0.14 for which thin-layer-cell behavior is observed for the peak current to within 5% for $\xi = \infty$. They arrived at this sweep-rate limit by comparing the relative magnitudes of the various terms in the one-dimensional, transient-diffusion equation. This limit agrees with what we found at small values of ξ, but it is over-restrictive at large ξ. That is, when the oxidized species concentration is initially dominant, the sweep rate can be over an order of magnitude higher than that given by Hubbard and Anson (6) and still have the cathodic peak current obtained from Eq. [15] to be within 5% of that obtained for LSV in a thin-layer cell.

The following empirical relationships, motivated by the asymptotic trends seen in Fig. 4, were fit to the peak currents and potentials obtained from Eq. [15]

$$I^*_{p,rev}(\sigma) = [I^*_{p,rev}(\text{planar})^m + I^*_{p,rev}(\text{thin-layer})^m]^{1/m} \qquad [20]$$

where

$$m = -0.565\left[\frac{\xi^{2.62}}{0.729 + \xi^{2.62}}\right] - 1.475 \qquad [21]$$

and

$$E^*_{p,rev}(\sigma) = [E^*_{p,rev}(\text{planar}) - E^*_{p,rev}(\text{thin-layer})]\left[\frac{\sigma}{m + \sigma}\right] + E^*_{p,rev}(\text{thin-layer}) \qquad [22]$$

where

$$m = 5.07\left[\frac{\xi^{2.68}}{1.98 + \xi^{2.68}}\right] + 2.13 \qquad [23]$$

The empirically determined m values from Eq. [21] and [23] were found by least squares fit of Eq. [20] and [22], respectively, to the dimensionless peak values for 51 values of σ ranging from 10^{-1} to 10^4 at each of 30 values of ξ ranging from 10^{-3} to 10^3. The functional dependence of m on ξ was obtained by using the empirically determined limiting m values at large and small ξ, and performing a two-parameter least square fit.

The error in the simulated voltammogram arising from the integral approximation given in Eq. [7] was assessed by comparing the peak currents obtained from Eq. [15] to those obtained from Eq. [16]. Although the peak current from Eq. [16] may be obtained by generating an entire voltammogram, a more convenient analytical procedure was derived by differentiating Eq. [16] with respect to τ and setting the result equal to zero. The potential which satisfies the resulting expression is the peak potential which, when substituted into Eq. [16], specifies the peak current. Newton's method was used to solve the resulting nonlinear equation for the peak potential generated from this procedure. For ξ ranging from 10^{-3} to 10^3 and σ varying from 10^{-1} to 10^4, the peak currents calculated from the two current-potential relationships agree to within 0.1% of each other, verifying the integral approximation in Eq. [7].

Methodology to determine the number of electrons transferred for a reversible reaction.—After Eq. [20] is made dimensional, the result indicates that plotting $(i_p/\nu)^m$ *vs.* $\nu^{-m/2}$ should yield a straight line with the slope or intercept given in Table V used to determine n, the number of electrons transferred. The "$\wedge$" symbol above the peak current indicates what would be measured if ohmic resistance and axial diffusion were negligible. The utility of this procedure was evaluated by choosing a set of values for all system variables, including n, using 30 simulation LSV data for which σ varied from 0.4 to 400, and then calculating n from the slope and the intercept. Table V lists the system

Table IV. Expressions for the peak current and potential on a planar electrode and in a thin-layer cell for reversible kinetics. The σ limit indicates the value at which the peak currents are within 5% and the peak potentials within 5/n mV (T = 298 K) of the values calculated for LSV in a cylindrical-pore electrode if ohmic resistance and axial diffusion are negligible.

Peak current or potential expression	Ref.	σ Limit
$I^*_{p,rev}(\text{planar}) = 0.6103 - 0.164\left(\frac{\xi}{1.08+\xi}\right)$	(5)	$\sigma > 300$
$E^*_{p,rev}(\text{planar}) = -\ln\left[\left(\frac{2.35}{\xi}\right)^{1.19} + 3.74\right]^{0.84}$	(5)	$\sigma > 40$
$I^*_{p,rev}(\text{thin-layer}) =$ $\xi \geq 1;\quad \frac{(1+\xi)\sqrt{\sigma}}{8\xi}$ $\xi \leq 1;\quad \frac{\sqrt{\sigma}}{2(1+\xi)}$	(6)	$\sigma < \exp\left[3.91\left(\frac{\xi}{0.59+\xi}\right) - 2.81\right]$
$E^*_{p,rev}(\text{thin-layer}) =$ $\xi \geq 1;\quad 0$ $\xi \leq 1;\quad \ln \xi$	(6)	$\sigma < 0.5$

variables, the calculated values of n, and the absolute percent deviation between the actual and calculated values. The majority of the data lie in the transition region between the planar-electrode and thin-layer-cell limits, and as expected the slope and the intercept give an estimate of n to within the same percent deviation. Due to the weak functional dependence of the peak potential on the sweep rate, the test for reversibility is best made by plotting the peak potentials as shown in the lower ordinate of Fig. 4.

Appreciable ohmic resistance with negligible axial diffusion.—Irreversible kinetics.—When ohmic resistance is appreciable, the potential is axially dependent, and the concentration and potential distributions must be determined simultaneously. The effect of ohmic resistance on the voltammogram when the kinetics are irreversible and axial diffusion is negligible was determined by simultaneously applying Eq. [10] and [13] with the pore divided into N segments. The current and potential in each segment are average values which vary with the segment location, and the coupled N current and N potential equations were iteratively solved using the IMSL nonlinear equation-solver subroutine DNEQNJ (22). The Filon algorithm (23) was used to perform the integration in Eq. [10], and a binomial averaging algorithm (24) was used to sum the infinite series. The total current was obtained by summing the individual segment currents at each time step.

In the limit of $\gamma \to \infty$, Eq. [10] is independent of γ. Further, for $\gamma \geq 10$ the peak current calculated by simultaneously applying Eq. [10] and [13] changed by less than 0.1% with γ. Therefore, when axial diffusion is negligible the voltammogram is not a function of γ for $\gamma \geq 10$; consequently, in the presence of appreciable ohmic resistance the voltammogram is a function of Λ, α, σ, and Θ (Fig. 1). Further, because Λ does not influence the magnitude of the peak current or the shape of the voltammogram but only the position of the peak potential relative to the formal potential, ohmic distortion can be quantified by examining the effect of α, σ, and Θ on the quantities $(I^*_{p,irrev}/\sqrt{\alpha})$ and $[\alpha E^*_{p,irrev} - \ln(\Lambda/\sqrt{\alpha})]$.

In the absence of ohmic resistance, the peak current and potential are a function of the product $\alpha\sigma$ with planar-electrode and thin-layer-cell behaviors occurring at large and small $\alpha\sigma$, respectively (Fig. 3). The degree to which Θ affects the voltammogram in the limit of large and small $\alpha\sigma$ is seen in comparing Fig. 5 and 6. For approximately a 20% decrease in the peak current relative to the case where ohmic resistance is negligible ($\Theta = 0$), a Θ value of 20 when $\alpha\sigma = 500$ (Fig. 5) is half that when $\alpha\sigma = 0.5$ (Fig. 6). Increasing Θ by 2.5 from $\Theta = 20$ to 50 and $\Theta = 40$ to 100 in Fig. 5 and 6, respectively, decreases the peak current in both voltammograms by another 20%. Therefore, in the transition from planar-electrode to thin-layer-cell behavior, Θ must increase to obtain the same percent decrease in the peak current. Although the percent decrease in the peak currents of the middle voltammograms in Fig. 5 and 6 is roughly equivalent, a $53/n\alpha$ mV ($T = 298$ K) shift in the voltammogram from the $\Theta = 0$ curve is seen in Fig. 5 but only an $18/n\alpha$ mV ($T = 298$ K) shift is seen in Fig. 6. Therefore, the shift in the peak potential is less pronounced than is the decrease in the peak current in moving from planar-electrode to thin-layer-cell behavior.

The voltammograms plotted in Fig. 5 and 6 result from simultaneously solving Eq. [2] and [5] using the IMSL finite-element solution PDE/PROTRAN (22) and then numerically integrating the Butler-Volmer kinetic expression (Eq. [3]) along the pore wall using the IMSL subroutine DQDAGS (22) at each time step. The reason this solution procedure was used is that the nonlinear equation solver failed to converge when ohmic resistance was substantial (greater than a 10% decrease in the peak current relative to the $\Theta = 0$ case). The finite-element solution, however, is a function of γ since the axial component of diffusion is included in Eq. [2]. In the next section we will discuss the effect of axial diffusion on the voltammogram and establish the criteria for which axial diffusion may be ignored. Unless otherwise stated, γ is large enough that the voltammograms reported in this section are independent of it.

Table V. The suggested manner to plot LSV data from a cylindrical-pore electrode for a reversible reaction in order to determine the number of electrons transferred. As an illustration, the agreement of simulation results with the empirical fit is presented assuming: $n = 1$, $T = 298$ K, $d = 0.02$ cm, $L = 0.3$ cm, $C^\circ_O = 10^{-5}$ mol/cm^3, $\mathcal{D} = 10^{-5}$ cm^2/s, and 0.25 mV/s $\leq \nu \leq$ 1 V/s. With this data, σ ranges from 0.4 to 400. The "∧" symbol above the peak current and potential indicates what would be measured if ohmic resistance and axial diffusion were negligible, and the empirical parameter m is given in Eq. [21].

Plot	$\left(\frac{\hat{i}_p}{\nu}\right)^m$ *vs.* $\nu^{-m/2}$
Slope	$(3.14nFdLC^\circ_O\sqrt{nf\mathcal{D}}I^*_p(\text{planar}))^m$
Intercept	
$\xi \geq 1$	$\left[\frac{0.196n^2fFd^2LC^\circ_O(1+\xi)}{\xi}\right]^m$
$\xi \leq 1$	$\left[\frac{0.785n^2fFd^2LC^\circ_O}{1+\xi}\right]^m$

ξ	n (Slope)	|%| Dev.	n (Intercept)	|%| Dev.
0.05	0.98	2	1.00	<1
1	0.98	2	0.96	4
20	0.99	1	0.99	1

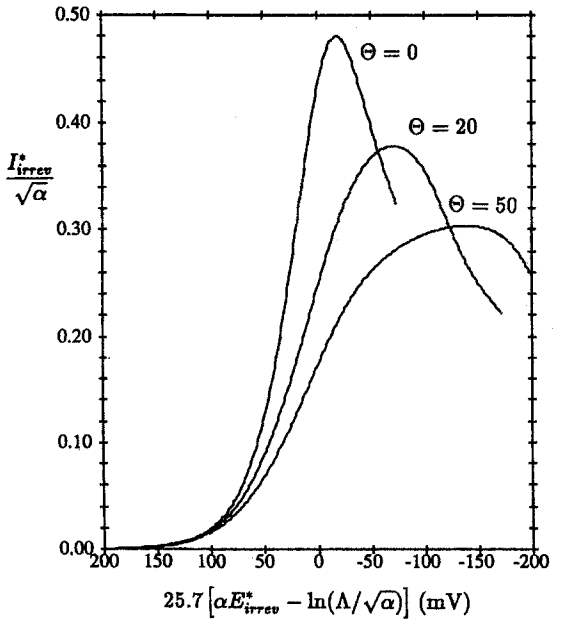

Fig. 5. Illustration of the effect of ohmic resistance on the calculated cathodic linear-sweep voltammogram in a cylindrical-pore electrode as the parameter Θ is varied. The simulations result from simultaneously solving Eq. [2] and [5] using the finite-element numerical solution with $\Lambda = 10^{-4}$, $\alpha = 0.5$, $\xi = 1.0$, $\sigma = 1000$, and $\gamma = 1000$. Under these conditions the kinetics are irreversible, planar-electrode behavior is approached, and axial diffusion is negligible.

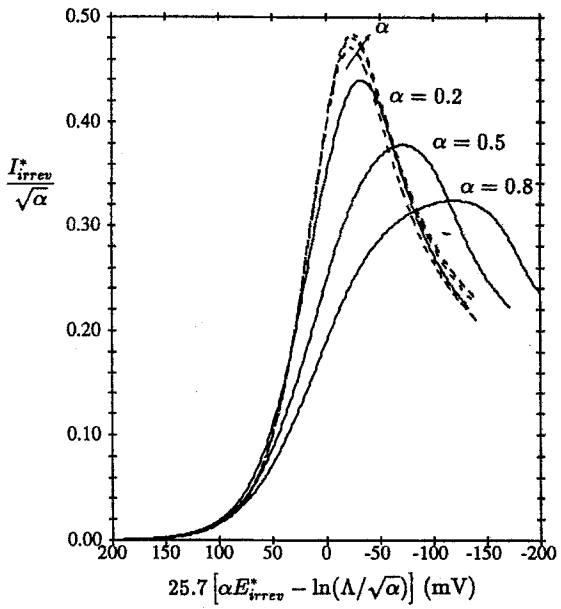

Fig. 7. Illustration of the effect of ohmic resistance on the calculated cathodic linear-sweep voltammogram in a cylindrical-pore electrode as the transfer coefficient α is varied. The solid curves result from simultaneously solving Eq. [2] and [5] using the finite-element numerical solution at Θ = 20 and γ = 1000, and the dashed curves result from Eq. [13] for which Θ = 0. All curves are for $\Lambda = 10^{-4}$, $\xi = 1.0$, and $\sigma = 1000$. Under these conditions the kinetics are irreversible, planar-electrode behavior is approached, and axial diffusion is negligible.

The degree to which α affects the ohmic distortion of the voltammogram is seen in Fig. 7 for ασ values at which planar-electrode behavior is approached. The dashed curves in the figure are the voltammograms at Θ = 0 which are weak functions of α. However, the decrease in the peak current and the shift in the peak potential in the presence of ohmic resistance are strong functions of α. As expected, ohmic distortion increases as α increases since the dimensional current increases.

The voltammogram is more sensitive to α than it is to Θ as seen by comparing Fig. 5 and 7. The middle solid curves in these two figures are identical (Θ = 20 and α = 0.5), and the effect of changing either Θ or α is observed by noting the percent decrease in the peak current and the shift in the peak potential relative to these curves. Increasing Θ from 20 to 50 (a 150% increase) or increasing α from 0.5 to 0.8 (a 60% increase) decreases both of the peak currents by approximately 20% and shifts both potentials by about $55/n\alpha$ mV (T = 298 K).

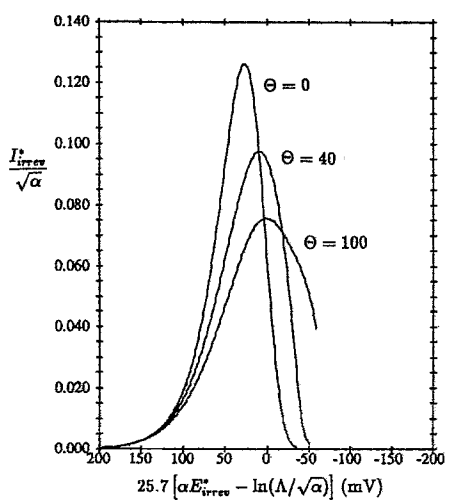

Fig. 6. Illustration of the effect of ohmic resistance on the calculated cathodic linear-sweep voltammogram in a cylindrical-pore electrode as the parameter Θ is varied. The simulations result from simultaneously solving Eq. [2] and [5] using the finite-element numerical solution with $\Lambda = 10^{-4}$, $\alpha = 0.5$, $\xi = 1.0$, $\sigma = 1$, and $\gamma = 1000$. Under these conditions the kinetics are irreversible, thin-layer-cell behavior is approached, and axial diffusion is negligible.

A convenient way to quantify the effect of ohmic distortion is to report the quantities $(I^*_{p,irrev}/\sqrt{\alpha})$ and $[\alpha E^*_{p,irrev} - \ln(\Lambda/\alpha)]$ relative to the case when ohmic distortion and axial diffusion are negligible. The resulting quantities are the normalized peak current $(i_p/\hat{i}_p)_{irrev}$, and the shift in the peak potential $\alpha(E^*_p - \hat{E}^*_p)_{irrev}$, where the "∧" symbol indicates the peak values that would be measured if ohmic resistance and axial diffusion were negligible. By systematically varying α, σ, and Θ, it was observed from the calculations that as $\sigma \to \infty$, $(i_p/\hat{i}_p)_{irrev}$ and $(E^*_p - \hat{E}^*_p)_{irrev}$ are proportional to $\alpha^{3/2}\Theta$, and as $\sigma \to 0$ both are proportional to $\alpha^2\Theta\sqrt{\alpha}$. An understanding of the functional dependence of ohmic distortion on these parameters in the planar-electrode and thin-layer-cell limits may be obtained by examining the magnitude of the decrease in the potential driving force along the length of the pore. The local potential driving force αE^* decreases down the pore due to the solution current. Therefore, the degree of ohmic distortion should be approximately proportional to the product of α times the characteristic potential drop given by the product of the total current i and the ohmic resistance in the pore R_s. In the planar-electrode limit the decrease in the dimensionless potential driving force can consequently be written as

$$\alpha nf(i \times R_s)_{planar} \to \alpha nf\left(nF\pi dLC^\circ_O(\alpha nfv\mathcal{D})^{1/2} \times \frac{L}{\pi(d/2)^2\kappa}\right) \quad [24]$$

which is proportional to $\alpha^{3/2}\Theta$. In the thin-layer-cell limit the same arguments result in

$$\alpha nf(i \times R_s)_{thin\text{-}layer} \to \alpha nf\left(n^2f F\pi(d/2)^2LC^\circ_O\alpha v \times \frac{L}{\pi(d/2)^2\kappa}\right) \quad [25]$$

which is proportional to $\alpha^2\Theta\sqrt{\sigma}$.

Not only are these two limits observed at large and small σ, but the transition in the limiting functional dependence of the peak current on α, σ, and Θ occurs over such a narrow σ range that a single plot of the simulated peak-current data may be obtained by dividing the results into two σ regions. Through trial and error, it was found that $(i_p/\hat{i}_p)_{irrev}$ is proportional to $\alpha^{3/2}\Theta$ to within ±2% for $\alpha\sigma \geq 1.75$, and this ratio is proportional to $\alpha^2\Theta\sqrt{\sigma}$ to within the same accuracy for $\alpha\sigma \leq 1.75$. Since by design $(i_p/\hat{i}_p)_{irrev}$ in these two regions are equal at $\alpha\sigma = 1.75$, a plot of $(i_p/\hat{i}_p)_{irrev}$ as a function of a single variable X_{irrev} is possible as shown in Fig. 8.

In order to correlate $(i_p/\hat{i}_p)_{irrev}$ to α, σ, and Θ, an empirical, three-parameter, least squares fit of the simulated peak currents shown in the upper portion of Fig. 8 was used to produce

$$(i_p/\hat{i}_p)_{irrev} = [(1.184 - 0.45 \log X_{irrev})^{-7.0} + 1]^{-1/7.0} \quad [26]$$

where X_{irrev} is defined in Fig. 8. It was observed from the calculations that the transition in the functional dependence of $\alpha(E_p^* - \hat{E}_p^*)_{irrev}$ on the governing parameters between the planar-electrode and thin-layer-cell limits occurred over a wider σ range than was seen with $(i_p/\hat{i}_p)_{irrev}$. To correlate the shift in the peak potential to the governing parameters, an empirical, two-parameter, least squares fit of the simulated peak potential results was used to produce

$$\alpha(E_p^* - \hat{E}_p^*)_{irrev} = aX_{irrev}^b \quad [27]$$

where

$$a = -5.7\left(\frac{\alpha\sigma}{9.4 + \alpha\sigma}\right) - 4.7 \quad [28]$$

and

$$b = 0.27\left(\frac{\alpha\sigma}{8.7 + \alpha\sigma}\right) + 0.58 \quad [29]$$

are empirical parameters which were found by least squares fit of Eq. [27] to $\alpha(E_p^* - \hat{E}_p^*)_{irrev}$ for 20 values of X_{irrev} at each of five values of ασ. The functional dependence of a and b on ασ was obtained by using the empirically known a and b values at large and small ασ, and performing a one-parameter least squares fit. Equations [26] and [27] were used to draw the solid lines in Fig. 8 and are seen to fit the calculations well. In order not to clutter the graph, Fig. 8 contains only peak potentials at the four indicated values of ασ.

The variable X_{irrev} reflects the trends seen in peak currents and potentials in Fig. 5-7. For instance, when σ decreases from 500 (Fig. 5) to 0.5 (Fig. 6), X_{irrev} is approximately constant at 7 by increasing Θ from 20 to 40. At a constant X_{irrev}, the normalized peak current is constant, but the shift in the peak potential from the Θ = 0 case decrease with ασ. In Fig. 5 and 7, the middle solid curves are identical with α = 0.5, σ = 1000, and Θ = 20 corresponding to a X_{irrev} = 7. Increasing Θ to 50 (Fig. 6) or α to 0.8 (Fig. 7) increases X_{irrev} to approximately 18 or 14, respectively, which corresponds to approximately a 35% decrease in the peak currents and a $110/n\alpha$ mV (T = 298 K) shift in the peak potentials for both voltammograms.

The "+" symbols representing the peak values in Fig. 8 are for σ varying from 0.1 to 1000, Θ from 0.01 to 300, and α from 0.1 to 0.9. The scatter in the symbols for a given X_{irrev} is due mainly to the slight functional dependence of $(i_p/\hat{i}_p)_{irrev}$ on σ for $\alpha\sigma \geq 1.75$. In this region, $(i_p/\hat{i}_p)_{irrev}$ goes through a minimum at $\alpha\sigma \doteq 10$ for a given Θ with $(i_p/\hat{i}_p)_{irrev}$ being within ±2% of that given Eq. [26]. Also, the peak currents and potentials are reported only for $X_{irrev} \leq 20$, since at that point the peak current has decreased 40% relative to the case of no ohmic resistance, and the peak potential shifted by as much as $130/n\alpha$ mV (T = 298 K) with the peak spread over tens of mV. The voltammogram shown in Fig. 5 for Θ = 50 is approaching this upper limit, and simulating and performing LSV beyond this point would be of little practical use.

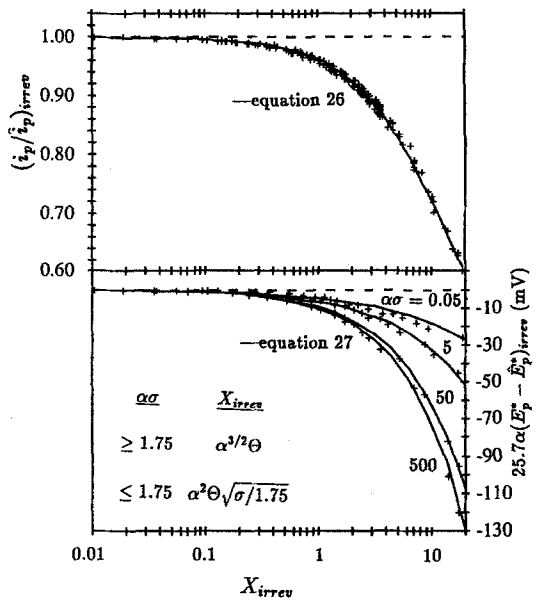

Fig. 8. The effect of ohmic resistance on the peak current and potential for linear-sweep voltammetry in a cylindrical-pore electrode as a function of X_{irrev} (see figure for definition) when the kinetics are irreversible and axial diffusion is negligible. The peak values are normalized by the results when ohmic resistance and axial diffusion are negligible, as indicated by the "∧" symbol. The "+" symbols result from either simultaneously applying Eq. [10] and [13] or from solving Eq. [2] and [5] using the finite-element numerical solution. The solid lines are the correlations that were fit to the peak values. The potential is for T = 298 K.

Methodology to extract kinetic constants for an irreversible reaction.—The goal of this work is to construct a method to extract kinetic constants from LSV measurements in a cylindrical-pore electrode as a model of a porous electrode. However, in order to plot the data as suggested in Table III, conditions must be such that axial diffusion may be ignored, and the effect of ohmic resistance taken into account. Ideally, one would operate in a region where axial diffusion is insignificant, and the measured peak current i_p would be divided by $(i_p/\hat{i}_p)_{irrev}$ (Eq. [26]) to obtain $\hat{i}_p$. Then α could be obtained from the average value of the slope and the intercept of a $(\nu/\hat{i}_p)^{1.81}$ *vs.* $\nu^{0.905}$ plot. However, the use of Eq. [26] requires the knowledge of α. Hence an iterative procedure is required in which an α value is guessed, Eq. [26] is applied, and the data analyzed via linear regression to determine a new α value from the slope and intercept given in Table III. If α(guessed) ≠ α(calculated) (where α(calculated) is the average of α determined from the slope and the intercept) then the guess is changed by setting α(guessed) = α(calculated), and the process is repeated until a desired convergence is achieved. Once the α value is determined, the standard rate constant k° may be obtained from the slope or intercept of a $(\nu e^{\alpha\hat{E}_{p,irrev}^*})^{2.05}$ *vs.* $\nu^{1.025}$ plot constructed as suggested in Table III in conjunction with Eq. [27].

The iterative procedure was tested by choosing a set of system variables, simulating eight voltammograms by simultaneously solving Eq. [2] and [5] using the finite-element numerical solution and applying the algorithm suggested above to extract the kinetic constants from the simulation results. Figures 9 and 10 show the peak current and potential results, respectively, plotted as suggested in Table III before and after the results were adjusted to account for solution resistance. The average α calculated was 0.412 which is 3% higher than the actual value of 0.4, and k° was 1.05×10^{-8} cm/s which is 5.0% too high. For this simulated data, X_{irrev} ranged from 2.1 to 47 and σ ranged from 0.39 to 195, which is in the transition region between the planar-electrode and thin-layer-cell limits. The slope and intercept yielded comparable kinetic constants, and in both cases the average of the two values resulted in the best estimate. The scatter in k° is significant and in prac-

tice the uncertainty in k° will probably be greater since the experimental uncertainty in the peak potentials is greater than the $\pm 1/n\alpha$ mV (T = 298 K) uncertainty in the simulations. However, the error is of the same magnitude as that arising from LSV on a planar electrode, and the resulting estimate of k° is usually sufficient.

Reversible kinetics.—The effect of ohmic resistance on the voltammogram when the kinetics are reversible was determined by simultaneously solving Eq. [2] and [5] using the finite-element solution procedure and numerically integrating the Butler-Volmer kinetic expression along the tube wall. A value for Λ was chosen which met the criteria for reversibility established by Matsuda and Ayabe (3) and Hubbard and Anson (8) for LSV on a planar electrode and in a thin-layer cell, respectively. A Λ value which ensures reversibility when ohmic resistance is negligible is valid in its presence since the effect of ohmic resistance is to decrease the local rate-of-change of the potential in the pore, facilitating equilibrium conditions at the pore wall.

The finite-element solution was used because the nonlinear equation solver, which was used in conjunction with Eq. [10] and [15], did not converge when ohmic distortion caused the peak current to decrease by more than 2% from that obtained when solution resistance is negligible. The finite-element solution is a function of γ since the axial component of diffusion is included in Eq. [2]. In the next section we discuss the effect of axial diffusion on the voltammogram and establish the criteria for which axial diffusion may be ignored. Unless otherwise stated, γ is large enough such that the voltammograms reported in this section are independent of it; consequently, in the presence of solution resistance, the voltammogram is a function of ξ, σ, and Θ (Fig. 1).

Investigating the effect of ξ, σ, and Θ on the voltammogram was computer intensive since only the finite-element solution was used. Evaluating the effect of the initial concentration ratio ξ on ohmic distortion was further complicated because time and spatial resolution had to increase as ξ decreased, since the concentration and potential gradients became steeper. For this reason, only extensive simulations were performed at $\xi \geq 100$ for which the peak current is less than 0.5% higher than at $\xi \rightarrow \infty$. The results may be valid at lower values of ξ since at $\xi = 20$ the peak current

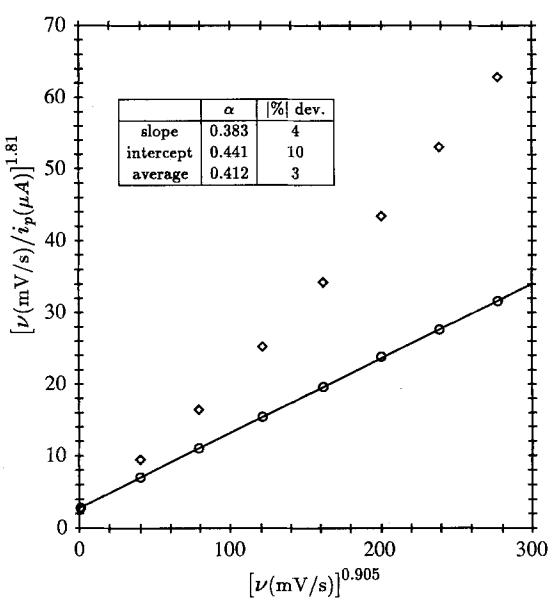

Fig. 9. Calculated peak-current results for LSV in a cylindrical-pore electrode obtained by simultaneously solving Eq. [2] and [5] (◇) and the results after they were adjusted to account for ohmic resistance using Eq. [26] (○). The following parameters were used in the calculations: n = 1, T = 298 K, d = 0.02 cm, L = 0.3 cm, $C\delta = 10^{-5}$ mol/cm³, $\mathcal{D} = 10^{-5}$ cm²/s, κ = 0.1 $(\Omega \cdot \text{cm})^{-1}$, α = 0.4, $k^\circ = 10^{-8}$ cm/s, and 1 mV/s $\leq \nu \leq$ 500 mV/s. The inset lists α and the absolute percent deviation from the actual value calculated from the slope and the intercept of the solid line, and the average of these two values.

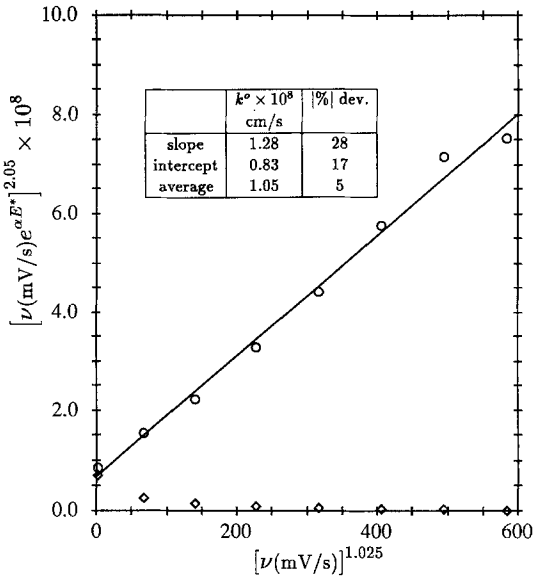

Fig. 10. Calculated peak-potential results for LSV in a cylindrical-pore electrode obtained by simultaneously solving Eq. [2] and [5] (◇), and the data after it was adjusted to account for ohmic resistance using Eq. [27] (○). The same parameter set reported in the caption of Fig. 9 was used. The inset lists k° and the absolute percent deviation from the actual value calculated from the slope and the intercept of the solid line, and the average of these two values. The average α value of 0.412 calculated in Fig. 9 was used to plot these data.

is only 2% higher than that at the infinite ξ limit, but results must be used with caution at lower ξ since at $\xi = 5$ and 1 the two peak currents differ by 7 and 20%, respectively.

By varying σ and Θ, it was observed from the finite-element calculations that as $\sigma \rightarrow \infty$, $(i_p/\hat{i}_p)_{rev}$ and $(E_p^* - \hat{E}_p^*)_{rev}$ are proportional to Θ, and as $\sigma \rightarrow 0$ they are proportional to $\Theta\sqrt{\sigma}$. Since the Nernst equation is applicable at the electrode surface, an understanding of the functional dependence of ohmic distortion at these two sweep-rate limits may be obtained by examining the decrease in the potential along the length of the pore. The magnitude of the potential decrease as planar-electrode and thin-layer-cell behavior are approached are given in Eq. [24] and [25], respectively, but with the α dependence eliminated.

The transition in the functional dependence $(i_p/\hat{i}_p)_{rev}$ on σ and Θ between the two sweep-rate limits occurs over a narrow σ range. Analogous to the case when the kinetics are irreversible, a functional dependence of $(i_p/\hat{i}_p)_{rev}$ on σ and Θ may be established by dividing the results into two σ regions. Through trial and error it was found that $(i_p/\hat{i}_p)_{rev}$ is proportional to Θ for $\sigma \geq 3.5$, and proportional to $\Theta\sqrt{\sigma}$ for $\sigma \leq 3.5$, both to within ±3%. Since by design $(i_p/\hat{i}_p)_{rev}$ in these two regions are equal at $\sigma = 3.5$, a plot of $(i_p/\hat{i}_p)_{rev}$ as a function of a single variable X_{rev} is possible and shown in Fig. 11.

In order to correlate $(i_p/\hat{i}_p)_{rev}$ to σ and Θ, an empirical, three-parameter, least squares fit of the simulated peak currents was used to produce

$$(i_p/\hat{i}_p)_{rev} = [(1.288 - 0.50 \log X_{rev})^{-7.0} + 1]^{-1/7.0} \quad [30]$$

where X_{rev} is defined in Fig. 11. It was observed that the calculated dependence of $(E_p^* - \hat{E}_p^*)_{rev}$ on the governing parameters between the planar-electrode and thin-layer-cell limits occurs over a wider σ range than was seen with $(i_p/\hat{i}_p)_{rev}$. To correlate the shift in the peak potential to the governing parameters, an empirical, two-parameter least squares fit of the simulated peak potentials was used to produce

$$(E_p^* - \hat{E}_p^*)_{rev} = aX_{rev}^b \quad [31]$$

where

$$a = -3.2\left(\frac{\sigma}{12.0 + \sigma}\right) - 8.2 \quad [32]$$

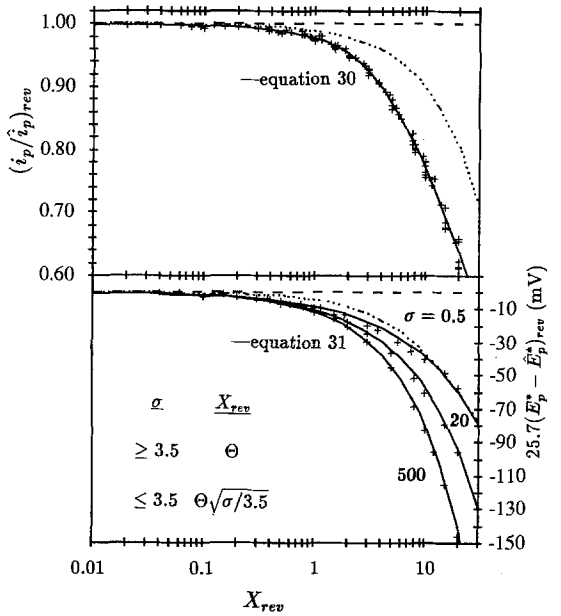

Fig. 11. The effect of ohmic resistance on the peak current and potential for linear-sweep voltammetry in a cylindrical-pore electrode as a function of X_{rev} (see figure for definition) when the kinetics are reversible and axial diffusion is negligible. The peak values are normalized by the results when ohmic resistance and axial diffusion are negligible as indicated by the "/\" symbol. The "+" symbols result from solving Eq. [2] and [5] using the finite-element numerical solution. The solid lines are the correlations that were fit to the peak values. The dotted lines are the correlations which were established for ohmic distortion in a thin-layer cell (25). The potentials are for $T = 298$ K.

and

$$b = 0.20\left(\frac{\sigma}{31.6 + \sigma}\right) + 0.66 \qquad [33]$$

are empirical parameters which were found by least squares fit of Eq. [31] to $(E_p^* - \hat{E}_p^*)_{rev}$ for 15 values of X_{rev} at each of eight values of σ. The functional dependence of a and b on σ was obtained by using the empirically known a and b values at large and small σ, and performing a one-parameter least squares fit. Equations [30] and [31] were used to draw the solid lines in Fig. 11 and are seen to fit the calculations well. In order not to clutter the graph, Fig. 11 contains only peak potentials at the three indicated values of σ.

The "+" symbols representing $(i_p\hat{i}_p)_{rev}$ in Fig. 11 are for σ varying from 0.5 to 500 and Θ from 0.01 to 300. The scatter in the calculated ordinates for a given X_{rev} is due mainly to the slight functional dependence of $(i_p/\hat{i}_p)_{rev}$ on σ for $\sigma \geq 3.5$. In this region, $(i_p/\hat{i}_p)_{rev}$ goes through a minimum at $\sigma \doteq 10$ for a given Θ with $(i_p/\hat{i}_p)_{rev}$ being within $\pm 3\%$ of that given by Eq. [30]. Also, peak currents and potentials are reported only for $X_{rev} \leq 20$ since at that point the peak current has decreased 40% relative to the case of no ohmic resistance, and the peak potential shifted by as much as $145/n\alpha$ mV ($T = 298$ K) with the peak spread over tens of mV. Simulating and performing LSV beyond this point would be of little practical use.

Also shown in Fig. 11 are the correlations we established in a previous publication for ohmic distortion of LSV in a thin-layer cell (25). Since Eq. [30] and [31] were shown to hold for σ as low as 0.5, they should be valid for thin-layer cells. Hinman *et al.* (26) used a resistor-network model to simulate LSV for reversible reaction kinetics in a thin-layer cell to account for ohmic distortion by making two assumptions in addition to the ones made in obtaining the results shown in Fig. 11: (*i*) the concentration and potential are radially uniform, and (*ii*) the rate at which the potential changes with time is uniform throughout the cell as set by the sweep rate. Using the same set of assumptions we applied a continuum model to the thin-layer cell (25), and found that the normalized peak current was a function of a single variable which in the present nomenclature is $\Theta\sqrt{\sigma}$. In order to plot the correlation from the thin-layer cell (25) in Fig. 11, a change in variables needs to be made where $\Theta\sqrt{\sigma/3.5} = X_{rev}$.

The correlation obtained for the thin-layer cell (25) and Eq. [30] predict a precipitous drop in the peak current as X_{rev} is increased past one, but the drop is steeper in the present calculations. For example, at $X_{rev} = 10$ the peak current calculated from the thin-layer model (25) is 17% higher than that calculated by numerically solving Eq. [2] and [5]. The calculated radial concentration and potential gradients were small for small σ; consequently, the difference in the peak currents predicted by the two models must result from assuming the sweep rate is uniform throughout the pore. As indicated by Eq. [19], the local current is not only a function of the axial-dependent potential, but it is also directly proportional to the local rate of change of the potential, $d|E|/dt$. Since $d|E|/dt$ decreases with distance into the pore, setting $d|E|/dt$ everywhere equal to the sweep rate ν overestimates the current. Since the peak potential in a thin-layer cell in the absence of ohmic resistance is independent of the sweep rate, the good agreement between the two peak-potential correlations at $\sigma = 0.5$ is not surprising.

Criteria for neglecting axial diffusion.—The correlation given in the previous section were obtained using peak values in which axial diffusion was assumed negligible. The degree to which axial diffusion affects the voltammogram increases as σ or γ decrease, since the slower the sweep or shorter the pore, the larger is the fraction of pore volume that will be affected by material diffusing into the pore. The influence of axial diffusion is also enhanced as Θ increases, since the reaction becomes more nonuniform and therefore the axial concentration gradients are steeper. To illustrate these trends, $(i_p/\hat{i}_p)_{irrev}$ and $(E_p^* - \hat{E}_p^*)_{irrev}$ are plotted in Fig. 12 as a function of σ for three values of Θ and γ when the kinetics are irreversible. The symbols result from simultaneously solving Eq. [2] and [5] which includes the axial component of diffusion, and the solid lines are the peak values obtained by simultaneously applying Eq. [10] and [13] in which the axial component of diffusion is not taken into account. No results are plotted in Fig. 12 for $\Theta > 10$ since the nonlinear equation solver would not converge for $\sigma > 3.5$.

When ohmic resistance is negligible ($\Theta = 0$), axial diffusion is only significant if material diffusing through the pore mouth contributes appreciably to the current. We see from the upper ordinate in Fig. 12 that at $\gamma = 10$, the normalized peak current is above unity at approximately $\sigma = 50$, but at $\gamma = 1000$ additional current due to the axial diffusion is not observed even at $\sigma = 1$. The symbols and lines do not exactly coincide at large σ and γ, but the difference is less than 0.5% and is believed to be due to numerical inaccuracy. The dependence of the peak potential on γ, shown in the lower ordinate of Fig. 12, is less noticeable. The differences between the symbols and the lines are due to numerical inaccuracy since the discrepancy is approximately equal to the size of the potential step used in the calculations ($1/n\alpha$ mV at $T = 298$ K).

In the presence of ohmic resistance, axial diffusion is enhanced due to the nonuniform potential distribution. The largest potential driving force occurs near the pore aperture where the reactant is replenished, accentuating the nonuniform current. From Fig. 12 we see that the contribution of axial diffusion to the peak current increases as Θ increases for a given σ and γ. For example, at $\sigma = 10$ the distance between the diamonds ($\gamma = 10$) and the squares ($\gamma = 100$) increases as Θ increases. The minimum in the peak current observed at $\sigma \doteq 10$ and $\Theta = 5$ and 10 is real and not just a numerical anomaly since both solution procedures indicate the trend. The lack of smoothness in the solid lines connecting the peak potentials at $\Theta = 5$ and 10, and the minimum observed at $\sigma = 500$ and $\Theta = 5$, is not believed to be real since the trends are within the size of the potential step used in the calculation.

The extensive simulations required to determine a detailed quantitative effect of γ on the voltammograms would be very computer intensive. Also, the results would

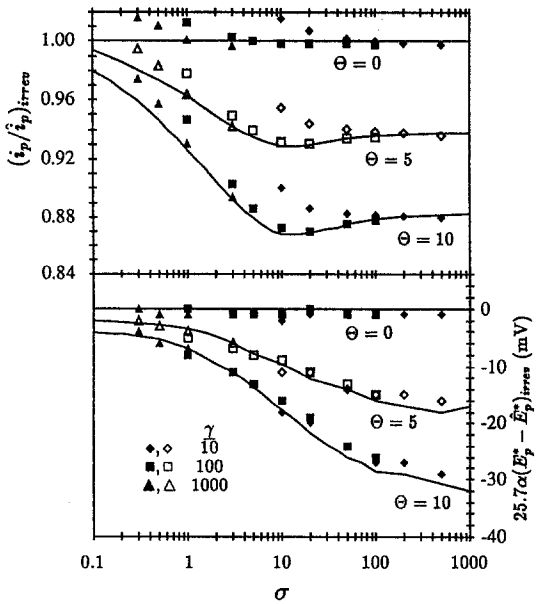

Fig. 12. Illustration of the effect of axial diffusion on the peak current and potential for linear-sweep voltammetry in a cylindrical-pore electrode as a function σ for three values of Θ and γ when the kinetics are irreversible and α = 0.5. The peak values are normalized by the case where ohmic resistance and axial diffusion are negligible as indicated by the "/\" symbol. The symbols and solid lines result from simulations with and without the axial component of diffusion included in the calculations, respectively. The potential is for T = 298 K.

be affected by the boundary conditions on the concentration field at the pore aperture. For these two reasons, such a parameter study was not conducted. However, simulations were performed to establish a rule-of-thumb estimate of when axial diffusion may be ignored for irreversible and reversible kinetics. When the kinetics are irreversible and ohmic resistance is negligible the peak currents calculated with and without the axial component of diffusion agreed to within 2% of each other as long as $\alpha\sigma > 40/\gamma$. The above criterion is valid in the presence of ohmic resistance for $X_{irrev} \leq 1$. For $X_{irrev} = 7$, the peak currents were independent of γ to within an error of 2% for $\alpha\sigma > 120/\gamma$, and at $X_{irrev} = 35$ the above conditions were satisfied when $\alpha\sigma > 400/\gamma$. This latter criterion was established before the limit on X_{irrev} of 20 was set for which LSV is not recommended since ohmic resistance grossly distorts the voltammogram. However, since the criterion is only a guideline, it can serve as a lower limit on ασ at a given γ for neglecting axial diffusion. The peak potential is less affected by γ over the parameter ranges studied here, and so the limits established to prevent axial diffusion from affecting the peak currents are adequate to ensure the peak potentials are not influenced.

When the kinetics are reversible and ohmic resistance is negligible, the peak currents were independent of γ to within an error of 2% as long as $\sigma > 40/\gamma$. The above criterion is valid in the presence of ohmic resistance for $X_{rev} \leq 1$. For $X_{rev} = 20$, the peak currents were independent of γ to within an error of 2% for $\sigma > 80/\gamma$, which serves as a lower limit on σ at a given γ for neglecting axial diffusion. Again, the limits established to prevent axial diffusion from affecting the peak currents are adequate to ensure the peak potentials are not influenced.

We may now comment on the effect γ may have had on the kinetic parameters determined from Fig. 9 and 10. The three lowest sweep rates on these figures for which $\alpha\sigma$ = 0.16, 9.2, and 19.6 all correspond to $X_{irrev} < 7$. As a conservative bound, with γ = 30, the sweep rate must be such that $\alpha\sigma > 120/30$, which is met by the last two points. For the other five sweep rates, X_{irrev} ranges from 7 to 12 requiring the criterion $\alpha\sigma > 400/30$ to be satisfied. Since ασ is greater than 20 for the five highest sweep rates, all voltammograms except the first are unaffected by axial diffusion. The one exception occurs at the lowest sweep rate where the actual current is 10% higher than that given by Eq. [26]. However, the α determined from Fig. 9 is unaffected by the error in this data point since the dimensional current at this lowest sweep is small compared to the currents at the higher sweep rates.

Summary

A pore in a porous matrix was modeled as a cylindrical-pore electrode, and the mass and charge conservation equations were solved in the context of this geometry when the potential at the pore aperture was ramped linearly in time. Both analytic and numeric techniques were used to solve the governing equations to account for the effects of ohmic, mass-transfer, and kinetic resistances. As outlined in Fig. 1, the peak currents and potentials obtained from the simulated voltammograms were correlated to the governing dimensionless parameters when axial diffusion was negligible. The correlations were used to establish a methodology for determining if the redox reaction kinetics are irreversible or reversible. If the reaction is irreversible, the standard rate constant and the transfer coefficient may be extracted from LSV data, and if the reaction is reversible the number of electrons transferred may be deduced. Also presented were the criteria for which axial diffusion and ohmic resistance may be ignored.

Table VI summarizes the correlations which were developed, the criteria for which the assumptions of negligible axial diffusion and/or ohmic resistance are valid, and the parameter range over which the correlations and criteria were established. The criteria correspond to the parameter value at which the assumption affected the peak current by less than 2%. Under these conditions, axial diffusion affects the peak potential by less than $1/n\alpha$ and $1/n$ mV (T = 298 K) for the irreversible and reversible kinetics, respectively. However, ohmic resistance can shift the peak as much as $10/n\alpha$ and $10/n$ mV (T = 298 K) in the irreversible and reversible kinetic limits, respectively, even though the peak current changes by only 2%. The shift in the peak potential is accounted for by applying either Eq. [27] or [31]. The methodology presented here to extract kinetic information should not rely on data which lie outside the parameter ranges given in Table VI. The restriction of $\gamma \geq 10$ is not severe since the shorter the pore the smaller is the value of X_{irrev} and X_{rev} (see Fig. 8 and 11 for the definitions), and the less is the resulting ohmic distortion. In the absence of ohmic resistance there is no restriction on γ as long as the criteria for neglecting axial diffusion are met. The limits on X_{irrev} and X_{rev} were set at a point at which ohmic distortion was so severe that LSV would be of little practical use, and $\xi \geq 100$ is in the region in which the voltammogram becomes independent of this parameter. Unless otherwise stated, the theoretical upper and lower limit on a particular parameter is infinity and zero, respectively. In practice the correlations could become invalid if such factors as double-layer charging, migration, or side reactions become a factor, all of which were not taken into consideration.

Acknowledgment

This work was supported by a grant from the NASA-Lewis Research Center (NAG 3-649). The majority of the computations were conducted using the Cornell National Supercomputing Facility. The authors would also like to thank The Electrochemical Society for recognizing this work by awarding John W. Weidner the 1989 Battery Division Student Research Award and the 1990 Energy Research Summer Fellowship funded by the U.S. Department of Energy.

Manuscript submitted Dec. 14, 1990; revised manuscript received Feb. 27, 1991.

LIST OF SYMBOLS

A	electrode area, cm^2
B_0	coefficient defined by Eq. [8]
B_μ	coefficient defined by Eq. [9]
C_O	concentration of oxidized species, mol/cm^3
C_R	concentration of reduced species, mol/cm^3
C_O^0	initial concentration of oxidized species, mol/cm^3

Table VI. A summary of the correlations which were developed in this work, criteria for which the assumptions are valid, and the parameter range over which the correlations and criteria were established. Unless otherwise stated, the upper and lower limit on a particular parameter is infinity and zero, respectively. X_{irrev} and X_{rev} are defined in Fig. 8 and 11, respectively, and the other dimensionless parameters are defined in Table I.

	Irreversible Kinetics		Reversible Kinetics	
Assume negligible axial diffusion (but with ohmic resistance)	Correlation equations: Peak current—17 and 26 Peak potential—18 and 27		Correlation equations: Peak current—20 and 30 Peak potential—22 and 31	
	$X_{irrev} \leq$	$\alpha\sigma >$	$X_{rev} \leq$	$\sigma >$
Criteria for neglecting axial diffusion	1	$40/\gamma$	1	$40/\gamma$
	7	$120/\gamma$	20	$80/\gamma$
	35	$400/\gamma$		
Valid parameter range	$\gamma \geq 10$ $X_{irrev} \leq 20$		$\gamma \geq 10$ $X_{rev} \leq 20$ $\xi \geq 100$	
Assume negligible axial diffusion and ohmic resistance	Correlation equations: Peak current—17 Peak potential—18		Correlation equations: Peak current—20 Peak potential—22	
Criteria for neglecting: ohmic resistance	$X_{irrev} \leq 0.53$		$X_{rev} \leq 0.91$	
axial diffusion	$\alpha\sigma > 40/\gamma$		$\sigma > 40/\gamma$	

C_R^0 initial concentration of reduced species, mol/cm³
C_O^* C_O/C_O^0
C_R^* C_R/C_O^0
d pore diameter, cm
$\mathcal{D}$ diffusion coefficient, cm²/s
E difference between the electrode and solution potentials, V
$E^{o'}$ formal potential, V
E_{eq} equilibrium potential, V
E^* dimensionless potential, $nf(E - E^{o'})$
$\hat{E}^*$ dimensionless potential when ohmic resistance and axial diffusion are negligible
f f/RT, V^{-1}
F Faraday's constant, C/equiv
h interval width in integral approximation
i total current, A
$\hat{i}$ total current when ohmic resistance and axial diffusion are negligible, A
I current density at electrode surface, A/cm²
I_0 zero-order modified Bessel function
I_1 first-order modified Bessel function
I^* dimensionless current density, $I/(nFC_O^0\sqrt{nf\nu\mathcal{D}})$
J_0 zero-order Bessel function
k^o standard rate constant, cm/s
L pore length, cm
n number of e^- in redox couple
N number of divisions in pore
R_s ohmic resistance of pore, Ω
R gas constant, J/(mol · K)
t time, s
T temperature, K
r distance from center of pore, cm
V volume of pore, cm³
X dimensionless parameter (see Fig. 8 and 11)
Y dimensionless radial coordinate, $2r/d$
z distance from the pore aperture, cm
Z dimensionless axial coordinate, $2z/d$

Greek

α cathodic transfer coefficient
β_n $(n - \frac{1}{2})\pi/\gamma$
γ length-to-radius ratio, $2L/d$
Θ $2n^{5/2}Ff^{3/2}L^2C_O^0(\nu\mathcal{D})^{1/2}/d\kappa$
κ conductivity of the electrolyte, $(\Omega \cdot cm)^{-1}$
λ_{n0} zeros of zero-order Bessel function J_o
λ_{n1} zeros of first-order Bessel function J_1
Λ $k^o/(nf\nu\mathcal{D})^{1/2}$
ν sweep rate, $-dE/dt$, V/s
ξ initial concentration ratio, C_O^0/C_R^0
σ $d^2nf\nu/4\mathcal{D}$
τ dimensionless time, $td^2/4\mathcal{D}$

Subscripts

irrev irreversible kinetics
p value at peak of voltammogram
qrev quasireversible kinetics
rev reversible kinetics
w value at tube wall

REFERENCES

1. A. J. Bard and L. R. Faulkner, "Electrochemical Methods," John Wiley & Sons, New York (1980).
2. P. Delahay, *J. Am. Chem. Soc.*, **75,** 1190 (1953).
3. H. Matsuda and Y. Ayabe, *Z. Electrochem.*, **59,** 494 (1955).
4. R. S. Nicholson and I. Shain, *Anal. Chem.*, **36,** 706 (1964).
5. J. W. Weidner and P. S. Fedkiw, *ibid.*, **62,** 875 (1990).
6. A. T. Hubbard and F. C. Anson, *ibid.*, **38,** 58 (1966).
7. A. T. Hubbard, *J. Electroanal. Chem.*, **22,** 165 (1969).
8. A. T. Hubbard and F. C. Anson, "Electroanalytical Chemistry," Vol. 4, A. J. Bard, Editor, pp. 129-214, Marcel Dekker, New York (1970).
9. A. Winsel, *Z. Elektrochem.*, **66,** 287 (1962). Translated by J. Newman, February, 1973. Available as Document No. UCRL-Trans-1495 from the National Technical Information Service, U.S. Department of Commerce, Front Royal, Virginia.
10. R. de Levie, "Advances in Electrochemistry and Electrochemical Engineering," Vol. 6, P. Delahay and C. W. Tobias, Editors, p. 329, Interscience, New York (1967).
11. M. D. Porter and T. Kiwana, *Anal. Chem.*, **56,** 529 (1984).
12. E. A. Grens, II and C. W. Tobias, *Ber. Bunsenges Phys. Chem.*, **68,** 236 (1964).
13. E. A. Grens, II and C. W. Tobias, *Electrochim. Acta*, **10,** 761 (1965).
14. E. A. Grens, *Electrochim. Acta*, **15,** 1047 (1970).
15. A. M. Bond, D. Luscombe, K. B. Oldham, and C. G. Zoski, *J. Electroanal. Chem.*, **249,** 1 (1988).
16. C. M. Bender and S. A. Orszag, "Advanced Mathematical Methods for Scientists and Engineers," McGraw Hill, New York (1978).
17. A. S. Viner and P. S. Fedkiw, *This Journal*, **137,** 1435 (1990).
18. F. B. Hildebrand, "Advanced Calculus for Applications," 2nd ed., Prentice-Hall, Englewood Cliffs, NJ (1976).
19. J. W. Weidner, Ph.D. Dissertation, North Carolina State University, Raleigh, NC (1991).
20. K. Aoki, D. Tokuda, and H. Matsuda, *J. Electroanal. Chem.*, **146,** 417 (1983).
21. L. Daruházi, K. Tokuda, and G. Farsang, *ibid.*, **264,** 77 (1989).
22. IMSL, "MATH/LIBRARY, FORTRAN Subroutines for Mathematical Applications," IMSL, Houston, TX (1987).
23. P. J. Davis and P. Rabinowitz, "Methods of Numerical Integration," Academic Press, New York (1975).
24. G. Dahlquist and Å. Björk, "Numerical Methods," Translated by N. Anderson, Prentice Hall, New York (1974).
25. P. S. Fedkiw and J. W. Weidner, *Electrochim. Acta*, **33,** 421 (1988).
26. A. S. Hinman, S. Pons, and J. Cassidy, *ibid.*, **30,** 89 (1985).